International Journal of Pharmaceutics 539 (2018) 1–10

Contents lists available at ScienceDirect

International Journal of Pharmaceutics

journal homepage: www.elsevier.com/locate/ijpharm

The relevance of shear, sedimentation and diffusion during spin freezing, as potential first step of a continuous freeze-drying process for unit doses

Joris Lammens[a], Séverine Thérèse F.C. Mortier[b,c], Laurens De Meyer[c], Brecht Vanbillemont[c], Pieter-Jan Van Bockstal[c], Simon Van Herck[a], Jos Corver[c], Ingmar Nopens[b], Valérie Vanhoorne[a], Bruno G. De Geest[a], Thomas De Beer[c,*,1], Chris Vervaet[a,1]

[a] Laboratory of Pharmaceutical Technology, Department of Pharmaceutics, Faculty of Pharmaceutical Sciences, Ghent University, Ottergemsesteenweg 460, 9000 Ghent, Belgium
[b] BIOMATH, Department of Mathematical Modelling, Statistics and Bioinformatics, Faculty of Bioscience Engineering, Ghent University, Coupure Links 653, 9000 Ghent, Belgium
[c] Laboratory of Pharmaceutical Process Analytical Technology, Department of Pharmaceutical Analysis, Faculty of Pharmaceutical Sciences, Ghent University, Ottergemsesteenweg 460, 9000 Ghent, Belgium

ARTICLE INFO

Keywords:
Freeze-drying
Shear
Sedimentation
Diffusion
Global sensitivity analysis
Uncertainty analysis

ABSTRACT

Recently, a continuous freeze-drying process for the production of unit doses was presented and evaluated. In this concept, the freezing step is modified compared to traditional batch freeze-drying, as glass vials filled with a liquid formulation, are rotated around their longitudinal axis while cooled and frozen with a cold, sterile and inert gas (i.e. spin freezing). Finally, a thin frozen product layer spread over the entire vial wall is achieved. The aim of this paper is twofold: firstly, the relation between the rotation velocity and the relative difference between top and bottom of the frozen product layer thickness was determined for different vial types. Secondly, the impact of shear and centrifugal forces generated during spinning was examined, to find out whether they might cause pharmaceutical instability and sedimentation, respectively. Mechanistic and experimental evaluation showed that shear has no effect on proteins. Calculations showed that the sedimentation and diffusion velocity is too low to cause inhomogeneity in the product layer. In addition, Global Sensitivity Analysis (GSA) and Uncertainty Analysis (UA) were performed in order to account for the uncertainty of the used mechanistic model.

1. Introduction

The pharmaceutical industry is 35 years after the approval of the first biopharmaceutical drug (i.e. recombinant human insulin) still confronted with several challenges during the development and manufacturing of biopharmaceuticals (Anne et al., 2012; Frokjaer and Otzen, 2005). One of the main challenges is the successful formulation of biopharmaceuticals (e.g. proteins), since biopharmaceuticals encounter stability issues when formulated as an aqueous solution (Frokjaer and Otzen, 2005; Franks, 1998; Pikal, 2002). Freeze-drying or lyophilisation is a low temperature drying process employed to convert these (heat-) labile solutions into solids of sufficient stability (Pikal, 2002). Glass vials, filled with an aqueous formulation, are placed on temperature controlled shelves. The temperature of these shelves is lowered to induce the formation of ice. During primary drying the formed ice crystals are removed under vacuum by sublimation. Lyophilisation ends with a secondary drying step, where the remaining unfrozen water is removed under vacuum by desorption. A solid dry cake with sufficient stability is obtained at the end of the cycle (Pikal, 2002; Wang et al., 2000; Kasper and Friess, 2011). Freeze-drying is traditionally performed in the pharmaceutical industry as a batch process. Nevertheless, several steps that precede freeze-drying as well as subsequent processes (i.e. filtering, filling steps, capping etc.), are already arranged in an efficient continuous way. As a result buffer systems, which are subjected to strict standards of cleanliness and sterility, are required which increases the production costs (De Meyer

* Corresponding author.
E-mail addresses: joris.lammens@ugent.be (J. Lammens), severine.mortier@ugent.be (S.T.F.C. Mortier), laurens.demeyer@ugent.be (L. De Meyer), brecht.vanbillemont@ugent.be (B. Vanbillemont), pieterjan.vanbockstal@ugent.be (P.-J. Van Bockstal), simon.vanherck@ugent.be (S. Van Herck), jos.corver@rheavita.nl (J. Corver), ingmar.nopens@ugent.be (I. Nopens), Valerie.Vanhoorne@UGent.be (V. Vanhoorne), br.degeest@ugent.be (B.G. De Geest), thomas.debeer@ugent.be (T. De Beer), chris.vervaet@ugent.be (C. Vervaet).
[1] Joint last author.

https://doi.org/10.1016/j.ijpharm.2018.01.009
Received 6 November 2017; Received in revised form 14 December 2017; Accepted 2 January 2018
Available online 31 January 2018
0378-5173/

Nomenclature

ΔL_{Rel}	maximum relative difference in average layer thicknesss (%)
$r_{v,i}$	inner radius of the vial (m)
$r_{p,i}$	radius from center of the vial to the border of the frozen product layer (m)
V_{fill}	filling volume (m^3)
h	height of the vial wall (m)
ω	rotation velocity ($m\,s^{-1}$)
τ	shear stress (Pa)
ν	viscosity of the solution ($kg\,m^{-1}\,s^{-1}$)
L	fluid layer thickness (m)
γ	shear rate (s^{-1})
d	distance (m) of a particle (e.g., macromolecule) to the axis of rotation
S_{max}	sedimentation coefficient (s)
M_w	molecular weight ($kg\,mol^{-1}$)
$v_{protein}$	partial specific volume of a protein ($m^3\,kg^{-1}$)
ρ	density of the used solvent ($kg\,m^{-3}$)
N_A	Avogadro's number (–)
R_{min}	minimum radius of a protein in solution (m).
α	acceleration ($m\,s^{-2}$)
$v_{sedimentation}$	sedimentation velocity ($m\,s^{-1}$)
D	diffusion constant
R	the gas constant ($8.314\,kg\,m^2\,s^{-2}\,K^{-1}\,mol^{-1}$)
T	Temperature (K)
M_b	buoyant mass (kg)
Si	actual fraction of variance accounted for by each factor (–)
S_{Ti}	sum of the first order effects and all interactions with other factors (–)

et al., 2015; Van Bockstal et al., 2016). Conventional batch freeze-drying also has several other disadvantages. The process is energy and time consuming, even an optimized cycle can last for days until a dry solid cake is obtained. In addition, like all batch processes, the process is liable to batch-to-batch variability (De Meyer et al., 2015; Van Bockstal et al., 2016). Moreover, the heat transfer inside a freeze-dryer is uneven. Vials at the edge of the shelves will dry faster than vials situated in the center due to radiative heat transfer from the warmer walls of the freeze-dryer. To circumvent all these disadvantages, a continuous freeze-drying process was recently presented and evaluated (Corver, 2013; De Meyer et al., 2015; Van Bockstal et al., 2016; Van Bockstal, 2016; De Meyer et al., 2017). The continuous freeze-drying concept also allows monitoring of each individual vial and provides therefore the opportunity to build and guarantee quality in each end product (unit dose) (US FDA, 2009). Furthermore continuous freeze-drying will offer a more flexible way of production, re-optimization for upscaling is no longer required when more product is demanded, this is simply done by running the process for a longer time or using parallel modules (De Meyer et al., 2015).

This study focuses on the spinning step (without freezing) of the continuous freeze-drying concept. Spinning is a part of the freezing step of the continuous freeze-drying concept. During this freezing step, vials, containing an aqueous drug formulation, are rotated around their longitudinal axis. Meanwhile, a flux of cold, inert and sterile gas is used for cooling and freezing. Hence, a thin frozen product layer equally spread over the entire vial wall is formed (i.e. spin freezing) (De Meyer et al., 2015; Van Bockstal et al., 2016). This approach reduces the product layer thickness and increases the surface area of the frozen product, allowing a significantly higher sublimation rate (up to a factor 40 or even higher (De Meyer et al., 2015; Van Bockstal et al., 2016)) compared to traditionally frozen vials in batch freeze driers. A difference in layer thickness between bottom and top of the vial would induce a difference in drying time, thus creating in-vial variability. In order to minimize this variability, the rotation velocity is determined in function of the relative difference in layer thickness between top and bottom of vial, from now on represented as ΔL_{Rel} to maintain the readability. Details about the drying process of this continuous freeze-drying process can be found in previous papers of our research group (De Meyer et al., 2015; Van Bockstal et al., 2016; Van Bockstal, 2016; De Meyer et al., 2017).

During spin freezing and before ice formation is initiated, the solution is rotated with a certain velocity, since it is dragged by the walls of the vial. The rotational velocity of the solution reduces towards the center of the vial (due to friction resulting from the viscosity of the fluid), creating a velocity gradient through the solution at the onset of rotation. This velocity gradient implies the existence of a shear rate through the solution, since shear rate is defined as the change of velocity from one fluid layer to another. Therefore, the dissolved biopharmaceuticals are subjected to potentially destabilizing shear forces. The influence of shear is examined in this paper via a mechanistic and experimental approach.

Another effect, resulting from the rotation of vials, is the generation of centrifugal forces. Each rotating object, is subjected to a force that is directed away from the axis of rotation. *Sensu stricto* is last mentioned force not a real force, but a consequence from inertia. Inertia is defined by Newton's first law: 'an object remains at rest or moves with a constant velocity, and in the same direction, unless an external force influences its movement'. However, inertia is the fundamental reason why centrifugation is capable to separate substances with a different density (Mok, 2006; Erickson, 2009; Cole et al., 2009). One of the aims of this paper is to examine if any relevant sedimentation can occur at the rotation velocities applicable for the continuous freeze-drying concept. It is not desired that sedimentation becomes relevant during spin freezing since it could cause for instance separation of the used stabilizer and active ingredient, which could lead to insufficient cryo- or lyoprotection and inhomogeneity in the frozen product layer. Besides sedimentation, diffusion could occur during spin freezing which could also induce inhomogeneity. Therefore, the sedimentation and diffusion velocity was calculated to determine the relevance of both phenomena during spin freezing.

2. Objectives

The relation between the rotation velocity during spin freezing and ΔL_{Rel} was determined for different vial types. In addition, the rotation velocity associated with a relative difference of 5% was determined in order to minimize intra-vial differences in drying.

Since spin freezing is inherently associated with rotation, a velocity gradient through the solution is formed, hence subjecting proteins to shear forces. The extent to which biopharmaceuticals are sensitive to shear-induced damage was first examined by a mechanistic approach and then verified with an experimental case study using alcohol dehydrogenase (ADH) as model protein. During this experimental study, the ADH activity was determined before and after rotation at different velocities, thus exposing ADH to different shear rates. In addition, dynamic light scattering (DLS) was used to compare the hydrodynamic diameter of ADH in solution before and after rotation, in order to detect possibly formed protein aggregates.

Another concern regarding spin freezing is the influence of the centrifugal forces that are generated. These forces could cause undesired separation of the stabilizers and biopharmaceuticals. The Relative Centrifugal Force (RCF), which causes sedimentation, was calculated in function of the applied rotation velocities. The sedimentation and diffusion velocity for typical biopharmaceucticals was

calculated in order to check the probability of inhomogeneity in the frozen product layer. In addition, GSA and UA was performed in order to account for the uncertainty of the calculations.

3. Methods and materials

3.1. Required rotation velocity

Spin freezing results in a thin frozen product layer spread equally over the entire inner vial wall. The thickness of the frozen product layer (L) can be calculated according to Eq. (1) (De Meyer et al., 2015; De Meyer et al., 2017; Van Bockstal et al., 2016; Van Bockstal, 2016). With, $r_{v,i}$ the inner radius of the vial (m), $r_{p,i}$ the radius from the center of the vial to the border of the frozen product layer (m), V_{fill} the filling volume (m^3) and h the height of the vial wall (m).

$$L = r_{v,i} - r_{p,i} = r_{v,i} - \sqrt{r_{v,i}^2 - \frac{V_{fill}}{\pi h}} \quad (1)$$

The relation between the rotation velocity (ω) and the difference in frozen product layer thickness (ΔL) between top and bottom of a vial is represented by Eq. (2) (De Meyer et al., 2015; De Meyer et al., 2017; Van Bockstal et al., 2016; Van Bockstal, 2016). Where ω is the required rotation velocity (rad s^{-1}), g the gravitational acceleration of the earth (9.807 m s^{-2}) and ΔL the difference in average frozen product layer thickness (m).

$$\omega = \sqrt{\frac{h\ g}{2\pi\ \Delta L\ r_{p,i}}} \quad (2)$$

Each vial type will require another rotation velocity in order to achieve the same relative difference in frozen product layer thickness, ΔL_{Rel} (in %), which is calculated according Eq. (3). The rotation velocities were calculated with the vial dimensions represented in Table 1. The relation between the rotation velocity and ΔL_{Rel} was calculated for each vial type. A filling volume of one fourth of the overflow capacity (i.e. the maximum filling volume of a vial when filled to the brim.) of each vial type is assumed when the required rotation velocity is calculated at different levels of envisaged ΔL_{Rel}. In addition the rotation velocity required to obtain a difference of 5% in ΔL_{Rel} is calculated.

$$\Delta L_{Rel} = \frac{\Delta L}{L} \quad (3)$$

3.2. Calculation of shear rate

Rotation of vials around their longitudinal axis causes a velocity gradient through the solution and might create shear stress on the solution components. The shear stress (τ) (Pa) developed during rotation was calculated by using Eq. (4), where ν is the viscosity of the solution (kg m^{-1} s^{-1}), ω the rotational velocity of a fluid layer (m s^{-1}) and L the fluid layer thickness (m). All fluids were assumed to be Newtonian in following calculations. Newtonian fluids are defined as fluids with a constant viscosity independently from the applied shear stress. This implies that for Newtonian fluids the shear rate (γ) (s^{-1}), corresponding with the applied τ, was calculated by Eq. (5). Each shear rate was calculated by assuming a viscosity of 1.519 10^{-3} kg m^{-1} s^{-1} (i.e. the viscosity of water at 278 K) and a fluid layer thickness calculated in according to Eq. (1). In some cases other solvents (e.g. tert-butanol) and higher concentrated solutions are used, which have a higher viscosity (i.e. 3.3 10–3 kg m-1 s-1 and up to 20 10–3 kg m^{-1} s^{-1} respectively). A higher viscosity result in a higher shear stress as defined by Eq. (4). It is important to realize that the shear rate was calculated assuming that the glass vial rotates at the required rotation velocity while the fluid layer at the vial wall was supposed to stand completely still. The latter assumption is therefore the most extreme case possible since the fluid at vial wall will not be completely immobile in reality. Moreover, the rotation velocity will be built up gradually before achieving the maximal rotation velocity, hence reducing the velocity difference between the fluid and the vial and thus reducing the shear rate.

$$\tau = \nu\ \frac{\omega}{L} \quad (4)$$

$$\gamma = \frac{\tau}{\nu} \quad (5)$$

3.3. Experimental setup

The influence of shear on the stability of proteins was verified with a case study where the activity of ADH was determined before and after rotation of the vials, and thus exposure to shear. Rotation of vials was carried out by placing them in an in-house build rotation device. No freezing was performed in order to separate shear stress resulting from vial rotation from freezing-induced stresses. Three 10 R type glass vials (Schott, Müllheim, Germany) were filled with 3 mL of a 1 mg mL^{-1}ADH solution. Each solution was subjected to a certain shear condition. The following shear conditions were evaluated: rotation of the vials at 2900 rotations per minute (rpm) for 2 min, 800 rpm for 4 min and 400 rpm for 4 min. In this way, the effect of exposure to high and low shear rates was studied for a short and longer time respectively. Afterwards the activity of the stressed ADH solutions is compared with the activity of a non-stressed 1 mg mL^{-1} ADH solution (i.e. the control solution). The assay was repeated 36 times for the control solution. All other shear conditions were evaluated in triplicate and the ADH assay was repeated 12 times for each replicate.

3.4. Preparation of ADH solution and ADH activity assay

A 1 mg mL^{-1} ADH solution prepared in 10 mM sodiumphosphate buffer (pH = 7.5) was used for all experiments. All solutions were, after exposure to shear, diluted with a 1 mg mL^{-1} bovine serum albumin solution (in 10 mM sodiumphosphate buffer) to 2.5 µg mL^{-1}, in order to get a concentration within the concentration range of the assay. A denatured negative control solution was prepared by heating a 1 mg mL^{-1} ADH solution for 30 min at 90 °C.

The activity of ADH was determined with an enzymatic assay (EC 1.1.1.1; adapted from Sigma Aldrich (modified for 96-well plates)) in a 96-well plate using a multimode plate reader (EnVision, Perkin Elmer, Zaventem, Belgium). The enzyme activity is expressed in units. One unit of ADH converts at 25 °C 1.0 μmol of ethanol to acetaldehyde per minute at pH 8.8. Sodiumpyrophosphate buffer (22 mM, pH = 8.8) is used to obtain the optimal pH during the enzyme assay. The assay is based on the rate of increase in absorbance at 340 nm caused by the formation of reduced β-Nicotinamide Adenine Dinucleotide (NADH) during the reaction. The concentration of NADH increases since β-Nicotinamide Adenine Dinucleotide (NAD^+) is reduced by ADH when ethanol is converted to acetaldehyde (Reaction given in Fig. 1). The increase of NADH concentration was monitored every 10 s during 6 min after adding the enzyme to the reaction medium.

Sodiumphosphate, ADH, bovine serum albumin and

Table 1
Dimensions of the different vial types used to calculate the required rotation velocity and the associated shear rates and relative centrifugal forces.

Vial size	Inner radius (mm)	Vial wall height (mm)	Overflow capacity (mL)
2R	7	22	4
4R	7	32	6
6R	10	26	10
8R	10	31	11.5
10R	11	30	13.5
15R	11	45	19
20R	13.5	35	26

$$CH_3CH_2OH + NAD^+ \xrightarrow{ADH} CH_3CHO + NADH$$

Fig. 1. ADH oxidizes ethanol to actaldehyde by reducing NAD^+.

sodiumpyrophosphate were purchased from Sigma–Aldrich (Saint Louis, Mo, USA). Ethanol was purchased from Fagron (Waregem, Belgium). 96 well-plates used for the assay were obtained from Novolab (Geraardsbergen, Belgium). The sensitivity of the assay was examined by making mixtures of denatured enzyme solution and non-denatured, non-stressed enzyme solution. In this way, solutions with 80, 50, 30 and 20 percent remaining activity were prepared. The measured activity of these solutions is compared with the theoretical activity. Each measurement is repeated 24 times. In addition, a denatured ADH solution was included as a negative control.

3.5. Dynamic light scattering

In order to control the formation of aggregates, the hydrodynamic diameter of ADH in solution was measured with DLS and compared before and after exposure to shear. DLS was performed on a Zetasizer Nano S (Malvern Instruments, Malvern, U.K.) equipped with a HeNe laser (λ = 633 nm) and detection at scattering angle of 173°. Data fitting by CONTIN was used to obtain the particle size distribution. All measurements were performed with a 1 mg mL^{-1} ADH solution and water as dispersion medium. Each measurement was done in triplicate.

3.6. Determination of the sedimentation and diffusion velocity

Centrifugal forces will also develop when a vial, filled with a solution of a biopharmaceutical formulation, rotates. These generated centrifugal forces can be presented as the RCF, which is expressed as multiples of the gravitational field of the earth (g = 9.807 m s^{-2}). The RCF was calculated by using Eq. (6) where d is the distance (m) of a particle (e.g., macromolecule) to the axis of rotation (i.e. the inner radius of the vial during spin freezing) and ω is the rotation velocity (rpm).

$$RCF = 11.18\ 10^{-2}\ d \left(\frac{\omega}{1000}\right)^2 \tag{6}$$

Biopharmaceuticals will start to sediment under these gravitational forces if their density is higher than the solvent density (Mok, 2006). The sedimentation velocity was calculated by making use of the sedimentation coefficient (S_{max})(s), which is defined as the ratio of the sedimentation velocity ($v_{sedimentation}$)(m s^{-1}) to the acceleration (α) (m s^{-2}) (i.e. the centrifugal field) as represented in Eq. (7) (Erickson, 2009; Le Roy et al., 2015; Cole et al., 2009).

$$S_{max} = \frac{v_{sedimentation}}{\alpha} = \frac{v_{sedimentation}}{d\ \omega^2} \tag{7}$$

Firstly the sedimentation velocity of proteins was determined. Therefore it is necessary to calculate the sedimentation coefficient, which depends on the size and shape of proteins as represented by the Svedberg equation (Eq. (8)) (Erickson, 2009; Le Roy et al., 2015). In Eq. (8) is M_w the molecular mass of the protein (kg mol^{-1}), $v_{protein}$ the partial specific volume of a protein (m^3 kg^{-1}), ρ the density of the used solvent (kg m^{-3}), ν the viscosity of the solvent (kg m^{-1} s^{-1}), N_A Avogadro's number and R_{min} the minimum radius of a protein in solution (m).

$$S_{max} = \frac{M_w(1-v_{protein}\ \rho)}{N_A\ 6\ \pi\ \nu\ R_{min}} \tag{8}$$

The sedimentation coefficient of ADH is determined as a case study in order to examine the relevance of sedimentation of proteins during spin freezing. Some assumptions were made to calculate S_{max} for ADH according Eq. (8). The first assumption concerns the volume V (m^3) that is occupied by a protein of molecular mass M_w (M_w = 150 kg mol^{-1} for ADH). The partial specific volume of the protein is needed to estimate this volume. ADH, has according to literature, an estimated partial specific volume ($v_{protein}$) of $0.73\,10^{-3}$ m^3 kg^{-1} (Erickson, 2009; Le Roy et al., 2015; Brown et al., 2011; Squire and Himmel, 1979; Harpaz et al., 1994).

$$V = \frac{M_w\ v_{protein}}{N_A} \tag{9}$$

ADH is a globular protein, which means that the tertiary structure of the protein is more or less spherical. This implies the possibility to calculate the minimal radius, by Eq. (10). Therefore it was assumed that the protein is perfectly spherical (Erickson, 2009).

$$R_{min} = \left(\frac{3V}{4\pi}\right)^{\frac{1}{3}} \tag{10}$$

Besides sedimentation, diffusion is also a phenomenon that occurs during the spin freezing step. The diffusion constant D (i.e. the diffusion velocity) is given by Eq. (11) (Erickson, 2009; Cole et al., 2009) where R is the gas constant (8.314 kg m^2 s^{-2} K^{-1} mol^{-1}) and T the temperature (K).

$$D = \frac{S_{max}\ R\ T}{M_w(1-v_{protein}\ \rho)} \tag{11}$$

Secondly, the sedimentation velocity of viruses is calculated. This was examined with a case study where the influenza virus was used as a model virus. Therefore the in literature experimental determined sedimentation coefficient was used (i.e. 700 Svedberg) (Lief and Henle, 1956; Friedewald and Pickels, 1944). Thirdly, the sedimentation velocity ($v_{sedimentation}$) of bacteria during spin freezing is determined. Eq. (8) requires some adjustments in order to calculate the sedimentation coefficient of bacteria since the partial specific volume ($v_{protein}$) and molecular weight (M_w) of bacteria are parameters that cannot be linked to bacteria. Eq. (8) is adjusted as represented in Eq. (12) by inserting the buoyant mass (M_b) of bacteria. The buoyant mass is defined by M_w (1-$v_{protein}$ ρ), therefore is the numerator of Eq. (8) substituted by the buoyant mass M_b of bacteria (Le Roy et al., 2015). For all calculations, a buoyant mass (M_b) ranging from $5\,10^{-18}$ kg to $800\,10^{-18}$ kg and a radius (R_{min}) of $2\,10^{-6}$ m was assumed. Similary, Eq. (11) was adjusted in order to calculate the diffusion constant (D) of bacteria and is represented in Eq. (13).

$$S_{max} = \frac{M_b}{6\ \pi\ \nu\ R_{min}} \tag{12}$$

$$D = \frac{S_{max}\ R\ T}{M_b} \tag{13}$$

3.7. Global sensitivity analysis and uncertainty analysis

The models to calculate S_{max} (Eq. (7)) and D (Eq. (11)) contain model parameters, which have an inherent uncertainty. In order to verify which of these model parameters has the most influence on the model output, i.e. S_{max} and D, a GSA was performed. Moreover, an UA was done to calculate the uncertainty on the model output. A sensitivity analysis is the study of how the uncertainty in the output of a model (numerical or otherwise) can be apportioned to different sources of uncertainty in the model input (or model structure, parameters) (Saltelli, 2006). Incentives to perform a sensitivity analysis are improving the understanding of the model behaviour, to facilitate model calibration, to perform model reduction, etc (Mortier et al., 2014). In the case of an uncertainty analysis, the outcome is the uncertainty on the output by propagating the uncertainties in the input variables. Both uncertainty and sensitivity analysis are important steps during model development.

Two sensitivity measures are calculated: the first order effect S_i and the total order effect S_{Ti}. S_i indicates the actual fraction of variance accounted for by each factor (Homma and Saltelli, 1996), whereas S_{Ti}

represents the total effect of factor *i*, i.e. the sum of the first order effects and all interactions with other factors. Different designs are known to calculate these sensitivity indices (McKay et al., 2000; Campolongo et al., 2011). The design proposed by Saltelli (2006) has been used (Mortier et al., 2014).

Both for the GSA as well as for the uncertainty analysis, Sobol sampling has been used to generate the input matrix (Saltelli, 2006). Both models contain seven uncertain parameters (Table 2). For both models 10,000 samples were used. The uncertainty for these parameters, used in the GSA is presented in Table 2. UA was performed for a worst case scenario, i.e. for the antibody Immunoglobulin M (IgM), which is the largest human antibody, and at the highest rotation velocity that will be used during spin freezing. The uncertainty for each parameter and the explanation for the chosen uncertainty is also represented in Table 2.

4. Results and discussion

4.1. Rotation velocity

The relation between ΔL_{Rel} and the rotation velocity was obtained according Eq. (2) and assuming a filling volume of one fourth of the overflow capacity. As represented in Fig. 2, a higher rotation velocity is associated with a smaller relative difference in frozen product layer thickness. Fig. 2 shows that 4R and 20R vials require the highest and lowest rotation velocity, respectively, in comparison with the other vial types. In agreement with Eq. (2), Fig. 2 indicates that vials with the same diameter, like 2R and 4R vials, strongly differ in required rotation velocity due to a different height of the vial wall. In Fig. 3, the influence of the filling volume on the rotation velocity is displayed for 10R vials. This figure illustrates that higher filling volumes allow lower rotation velocities to obtain the same maximum relative difference. It is worthwhile to realize that the rotation velocities in Fig. 2 are calculated for filling volumes of one fourth of the overflow capacity of each vial. For higher filling levels, even lower rotation velocities are allowed to obtain the same relative differe on the frozen product layer thickness. The thickness of the frozen product layer has an important influence on the drying time since a thicker frozen product layer leads to longer drying times. The rotation velocity to obtain a ΔL_{Rel} of 5% is displayed in Table 3. Table 3 also presents the shear rates and relative centrifugal forces calculated according to Eq. (5) and (6), respectively. A filling volume of one fourth of the overflow capacity was used for the calculations of the RCF and shear rates. The effect of these parameters will be evaluated in the next sections of the paper. A ΔL_{Rel} of 5% was chosen since lower relative differences in layer thickness could lower the practical feasibility of spin freezing. In addition, lower relative differences in layer thicknesses between top and bottom of the vial would cause only marginal differences in drying time between top and bottom of the frozen product layer.

4.2. Generated shear rates

As described in Section 4.1 higher rotation velocities are associated with smaller differences in the frozen product layer thickness. However, higher rotation velocities generate, according to Eqs. (4) and (5), higher shear rates. The relation between the generated shear rate and ΔL_{Rel} is represented in Fig. 4 for different vial types. Fig. 4 illustrates that the shear rate increases when a lower ΔL_{Rel} is envisaged, due to the higher required rotation velocity. As described in Section 4.1 a ΔL_{Rel} of 5% is generally desired. The required rotation velocities and associated shear rates are represented in Table 3.

4.3. Theoretical verification and discussion of the influence of shear during spin freezing

One of the aims of this paper was to examine the relevance of the shear forces, generated during spin freezing, on the stability of biopharmaceuticals. As mentioned earlier, the shear rate was calculated assuming that the glass vial rotates at the required rotation velocity while the fluid layer at the vial wall was supposed to stand completely still. The latter assumption is therefore the most extreme case possible since the fluid at vial wall will not be completely immobile in reality. However, even in this worst case scenario, all calculated shear rates are comparable or even lower compared to the shear rates developed during other typically upstream process steps applied during the manufacturing of biopharmaceuticals, as shown in Table 4. These processes are generally accepted without questioning the impact of these shear rates on the stability of the processed biopharmaceuticals. Even the shear rates associated with rotation velocities to obtain a ΔL_{Rel} of 2%, represented in Fig. 4, are comparable with shear rates during other standard pharmaceutical production processes represented in Table 4. The effect of shear forces on protein stability is a topic of interest in literature (Brückl et al., 2016; Maa and Hsu, 1997; Bee et al., 2009; Jaspe and Hagen, 2006; Virkar et al., 1981; Oliva et al., 2003; Kroll, 1996; Stroev et al., 2007; Bekard and Dunstan, 2009; Colombie et al., 2001; Thomas and Dunnill, 1979). Bee et al. (2009) compared the force required to unfold a protein with the force applied to proteins by exposure to shear. Atomic force microscopy experiments pointed out that a force of about 20 and 150 pN is required to cause unfolding of α -helical and β -sheet proteins respectively. Bee et al. (2009) stated that for a 10.5 nm monoclonal antibody, the applied shear force is 0.06 pN when a shear rate of 20,000 s^{-1} is applied to a solution with $\nu = 3$ kg m^{-1} s^{-1}. 0.06 pN is multiple orders of magnitudes lower than the force needed to unfold proteins (Bee et al., 2009).

Bee et al. (2009) calculated that a shear rate of $5\,10^{7}$ s^{-1} is required to achieve a force of 150 pN on a protein (Bee et al., 2009) (i.e. the force required to cause unfolding of the protein). This shear rate is much higher compared to common shear rates in pharmaceutical processes given in Table 4 and to the highest shear rate that will be obtained during spin freezing. The rotation velocity that would be required to achieve this shear rate can be calculated by Eq. (4) and (5). When a dynamic viscosity of $1.519\,10^{-3}$ kg m^{-1} s^{-1} (i.e. the viscosity of water at 278 K) and a layer thickness of 2 mm is assumed, a rotation velocity of $8.6\,10^{7}$ rpm is required to achieve the shear rate that could cause protein unfolding according to Eq. (4) and (5).

Bee et al. (2009) stated that the estimated force resulting from surface tension at the air-water interface is 140 pN when a water surface tension of 0.07 N m^{-1} is assumed. This suggests that the force resulting from surface tension is more likely to cause protein damage than the applied shear forces (Bee et al., 2009).

Thermodynamics also indicate that unfolding of proteins is more likely a result of adsorption to air-water surfaces than of shear forces.

Table 2
Nominal values for the different parameter affecting sedimentation and diffusion used for GSA and UA. The nominal values for the UA are given between brackets if they differ from the values used for GSA.

Parameter	Minimum	Maximum	Explanation for selected interval
$v_{protein}$ (m^3 g^{-1})	$0.70\,10^{-3}$	$0.75\,10^{-3}$	Data Literature (Brown et al., 2011; Squire and Himmel, 1979; Harpaz et al., 1994)
M_w (kg mol^{-1})	15(890)	900(910)	Typical molecular weights for proteins
ρ (kg m^{-3})	990.8	998.2	Density of water at 293 and 273 K respectively
ν (kg m^{-1} s^{-1})	$1.016\,10^{-3}$	$1.79\,10^{-3}$	Viscosity of water at 293 and 273 K respectively
d (m)	$0.7\,10^{-2}$	$1.35\,10^{-2}$	Possible radii for vials (from 2R up to 20R vials)
rpm	500(9176)	9181(9186)	Settings rotation velocity
T (K)	273	293	Temperature range during spin freezing

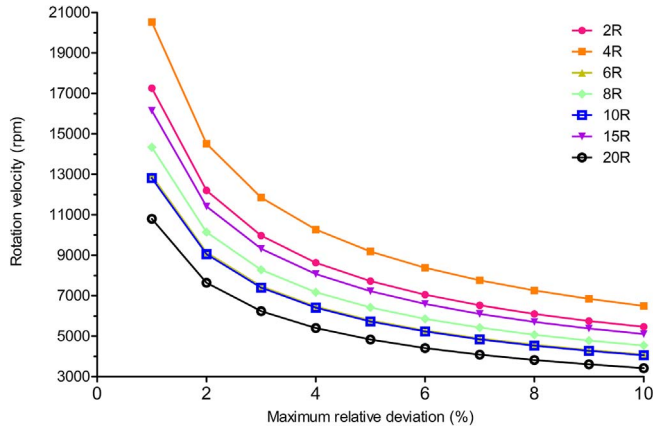

Fig. 2. The rotation velocity in function of a maximum relative difference on the product layer thickness for different vial types: 2R (pink), 4R (orange), 6R (yellow), 8R (green), 10R (blue), 15R (purple), 20R (black). (For interpretation of the references to colour in this figure legend, the reader is referred to the web version of this article.)

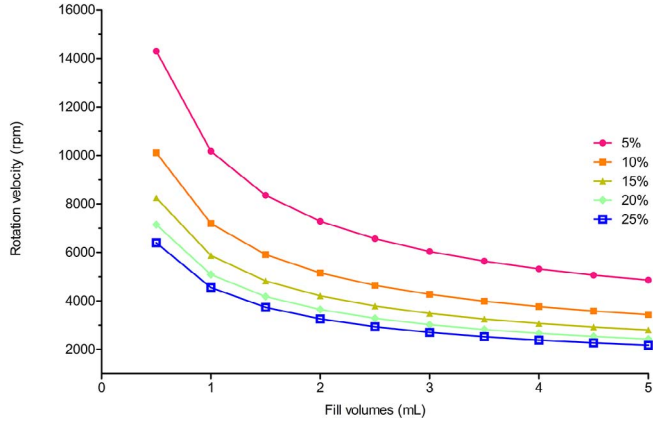

Fig. 3. The rotation velocity to obtain a certain ΔL_{Rel} for 10R vials in function of the filling volume. 5% (pink), 10% (orange), 15% (yellow), 20% (green), 25% (blue). (For interpretation of the references to colour in this figure legend, the reader is referred to the web version of this article.)

Table 3
Different vial types with the required rotation velocity to obtain a maximum difference on the layer thickness of 5% and their associated shear rates and relative centrifugal forces.

Vial Type	Required rotation velocity (rpm)	Shear rate (s^{-1})	RCF (g)
2R	7717	5034	466
4R	9181	5791	660
6R	5780	3625	374
8R	6413	4184	460
10R	5729	3728	404
15R	7218	5035	641
20R	4829	2982	360

The difference in free energy between the folded and unfolded state explains the thermodynamic stability of globular proteins. For a globular protein this difference in free energy is about $5\,10^{-20}$ J per molecule (Thomas and Geer, 2011). This change in free energy can be compared with the energies resulting from exposure to shear and adsorption to air-water surfaces. When a shear stress of 1 Pa is applied on a globular protein, a deformation energy of about 10^{-25} J is developed (Walstra et al., 2001; Thomas and Geer, 2011. Thomas and Geer (2011) stated that this suggests that a shear stress of about $5\,10^{5}$ Pa is required to denature a globular protein, which is equivalent with a shear rate of $5\,10^{8}$ s^{-1} for aqueous globular protein solutions (Thomas and Geer, 2011). This is again far higher than shear rates that will be developed

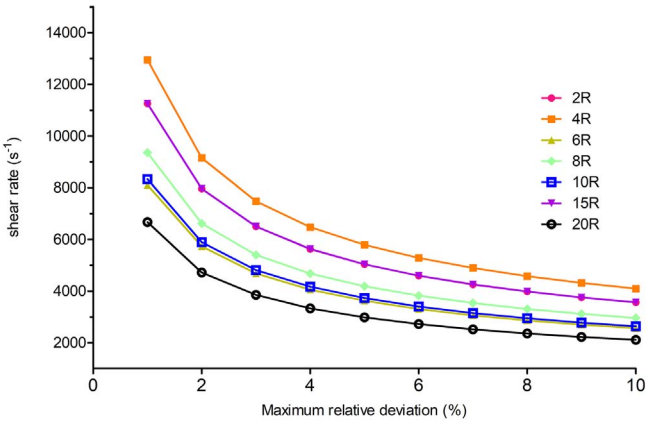

Fig. 4. The generated shear rate associated with the rotation velocity to obtain a certain ΔL_{Rel} for different vial types: 2R (pink), 4R (orange), 6R (yellow), 8R (green), 10R (blue), 15R (purple), 20R (black). (For interpretation of the references to colour in this figure legend, the reader is referred to the web version of this article.)

during spin freezing. In contrast, it is stated that the energy resulting from adsorption to the air-water surface is 10^{-18} J per molecule (Thomas and Geer, 2011) and is therefore more relevant for globular protein denaturation than the deformation energy resulting from shear stress. This emphasizes the role of air-water surfaces in protein stability. In addition to the above discussed theoretical concepts, literature holds several experimental findings that support these theoretical concepts. Brückl et al. (2016) observed no changes in secondary and tertiary structure of Recombinant Human Growth Hormone (rhGH) and immunoglobulin G1 when exposed to shear rates of $3840\,s^{-1}$ (Brückl et al., 2016).

In contrast irreversible and time-dependent unfolding of rhGH was observed when subjected without surfactant to shear forces in a Couette cell in the presence of air bubbles (Brückl et al., 2016). A similar conclusion is made by Maa and Hsu (1997), studying the stability of rhGH and Recombinant Human Deoxyribonuclease (rhDNase) under high shear rates in the presence of air-liquid interfaces. No major effect on the stability of rhDNase could be seen, but rhGH formed non covalent aggregates. The formation of these aggregates increased with an increasing interfacial area. In addition, they observed that the formation of aggregates could be delayed or avoided by adding a surfactant. The effect of air-liquid interfaces was also studied in low-shear conditions by foaming the solution with nitrogen. It became clear that foam has a strong adverse effect on the stability of rhGH. The stability of rhGH increased again when anti-foaming materials were added to the solution (Maa and Hsu, 1997). An other study examined the effect of shear on the stability of Bovine Serum Albumine (BSA) and Human Serum Albumine (HSA) (Oliva et al., 2003). BSA and HSA showed to have different aggregation kinetics under the same shear rates. These differences could be explained by their different affinity for the air-water interface, since the amount of shear and the available air-water surface are considered as fixed factors (Oliva et al., 2003). This also suggested that adsorption to air-water interfaces cannot neglected in shear studies. Virkar et al. (1981) observed no loss of activity when ADH is subjected to shear in a completely filled rotating-disk reactor. But when the reactor was filled incompletely an activity loss of 60% is observed after 5 h. They concluded that secondary effects such as interfacial denaturation must be considered (Virkar et al., 1981).

Bee et al. (2009) subjected immunoglobulin G1 to shear rates up to $2.5\,10^{5}$ s^{-1} in a parallel plate and a capillary rheometer. Even at very high shear rates, no detrimental effects on the structure of the protein could be observed (Bee et al., 2009). Cytochrome C was subjected to shear rates as large as $2\,10^{5}$ s^{-1}, no evidence was found that these shear rates could destabilize cytochrome C (Jaspe and Hagen, 2006). In addition, the authors proposed a model for proteins in a simple shear flow

Table 4
Typical shear rates in pharmaceutical industry and biological processes.

Pharmaceutical or biological process	Estimated associated shear rate (s^{-1})	Exposure time	References
Mixing processes	50	Up to several hours	(Bee et al., 2009)
Pipe Flow	2000	Seconds	(Bee et al., 2009)
Cross-flow filtration	1000–10,000	Seconds	(Davis, 2001)
Filling operations (20 gauge needle)	20,000	Milliseconds	(Wilkes, 2006)
Pulsatile blood flow in the arterial system	1640–10,000	N/A	(Kroll, 1996; Stroev et al., 2007)
Lobe Pumps	16 000–20 000	Seconds (multiple times)	(Gomme et al., 2006)

Table 5
Comparison of measured and expected activities of ADH solutions.

	Actvity (units mg^{-1})	SD (units)	Expected actvity (units mg^{-1})	Deviation (%)
Control solution	109.04	6.49	N/A	N/A
80 %	88.43	4.43	87.23	1.35
50 %	50.10	5.01	54.52	8.11
30 %	32.21	2.40	32.71	1.52
20 %	21.67	1.06	21.80	0.60
Denatured solution	−1.31	0.82	0	N/A

Table 6
ADH activity after exposure to different shear rates.

	Corresponding shear rate (s^{-1})	Actvity (units mg^{-1})	Standard deviation (units)
Control solution	0	109.04	6.49
2900 rpm (2 min)	2145	110.06	11.22
800 rpm (4 min)	591	112.42	8.11
400 rpm (4 min)	295	109.26	8.04

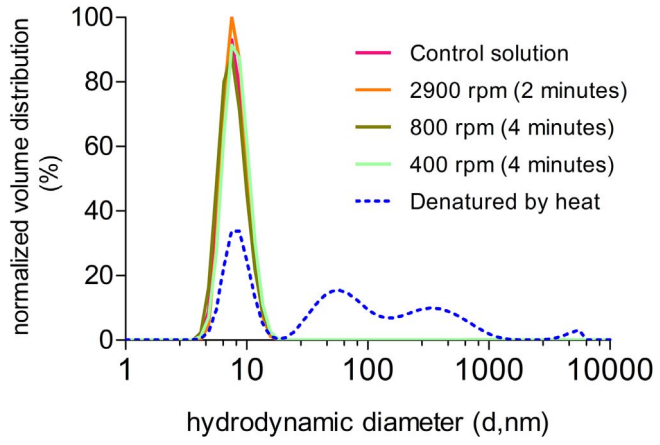

Fig. 5. Normalized volume distribution curves of the hydrodynamic diameter of ADH measured by dynamic light scattering, before and after exposure to different shear rates. No difference in size could be observed for any applied shear rate in comparison with a control solution.

that suggested that shear rates in the order of 10^7 s^{-1} would be required to cause any damage to small globular proteins.

However, literature does contain some reports of shear related damage, when proteins are subjected to shear (Bekard et al., 2011; Bekard and Dunstan, 2009; Singh et al., 2009; Ashton et al., 2009). In most of these cases the exposure time is in the order of multiple hours and therefore not pertinent for the duration of spin freezing.

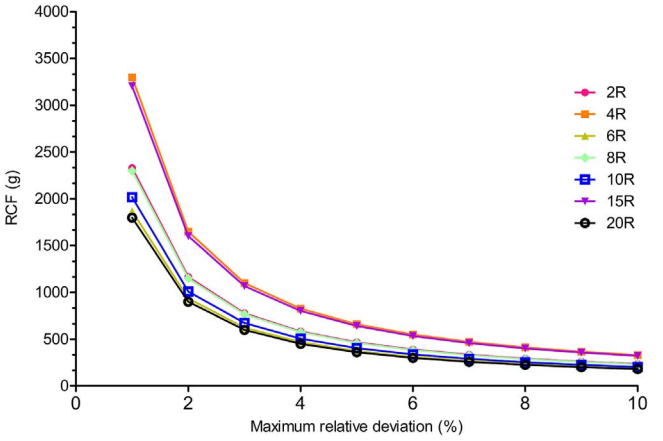

Fig. 6. The generated RCF associated with the rotation velocity to obtain a certain ΔL_{Rel} for different vial types: 2R (pink), 4R (orange), 6R (yellow), 8R (green), 10R (blue), 15R (purple), 20R (black). (For interpretation of the references to colour in this figure legend, the reader is referred to the web version of this article.)

Table 7
Sedimentation velocity for bacteria for the rotation velocity to obtain a ΔL_{Rel} of 5%.

	4R vial	20 R vial
Required rotation velocity (rpm)	9181	4829
v_{sed} for *Mb* of 5 10^{-18} kg (m s^{-1})	8.57 10^{-7}	4.5 10^{-7}
v_{sed} for *Mb* of 800 10^{-18} kg (m s^{-1})	1.37 10^{-4}	7.21 10^{-5}

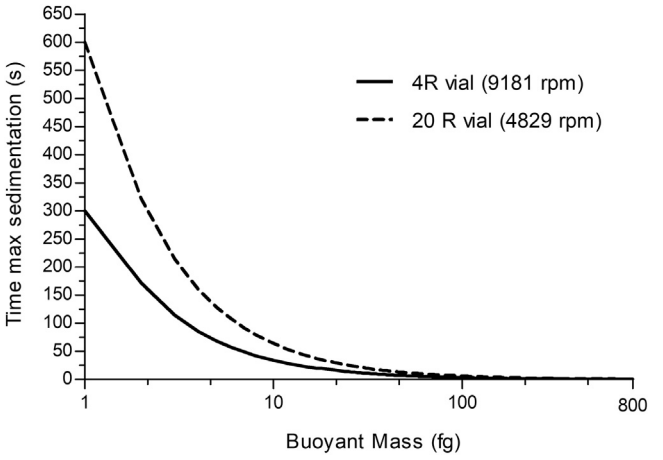

Fig. 7. The required time to reach the maximum allowed sedimentation distance which causes a maximum frozen product layer inhomogeneity of 5% for different buoyant masses, for 20R vials and 4R vials.

4.4. Experimental verification

4.4.1. Sensitivity of the assay

The sensitivity of the assay was determined by making mixtures of a denatured ADH enzyme solution and a non-denatured, non-stressed

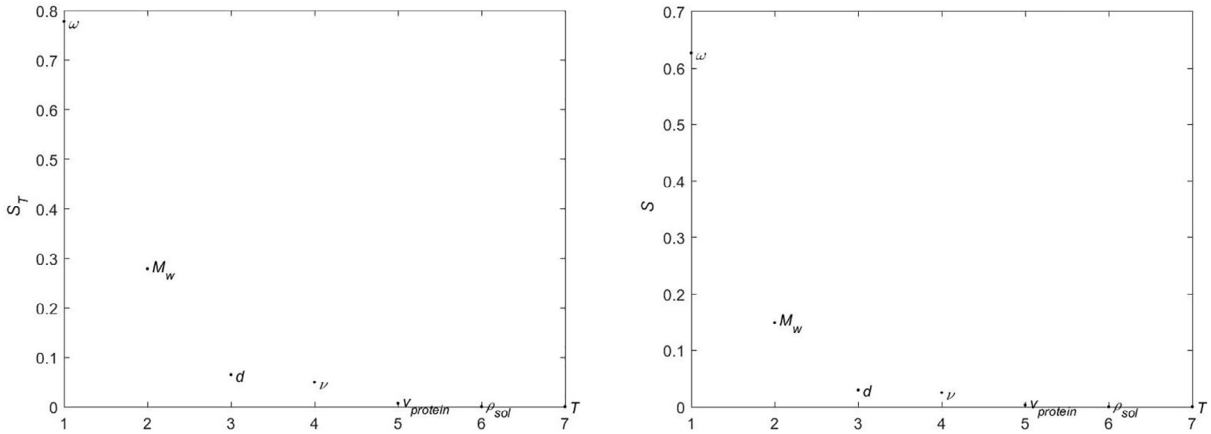

Fig. 8. GSA results for the sedimentation velocity: *Si* (Right) and S_{Ti} (Left). *Si* indicates the actual fraction of variance accounted for by each factor (Homma and Saltelli, 1996), whereas S_{Ti} represents the total effect of factor *i*, i.e. the sum of the first order effects and all interactions with other factors.

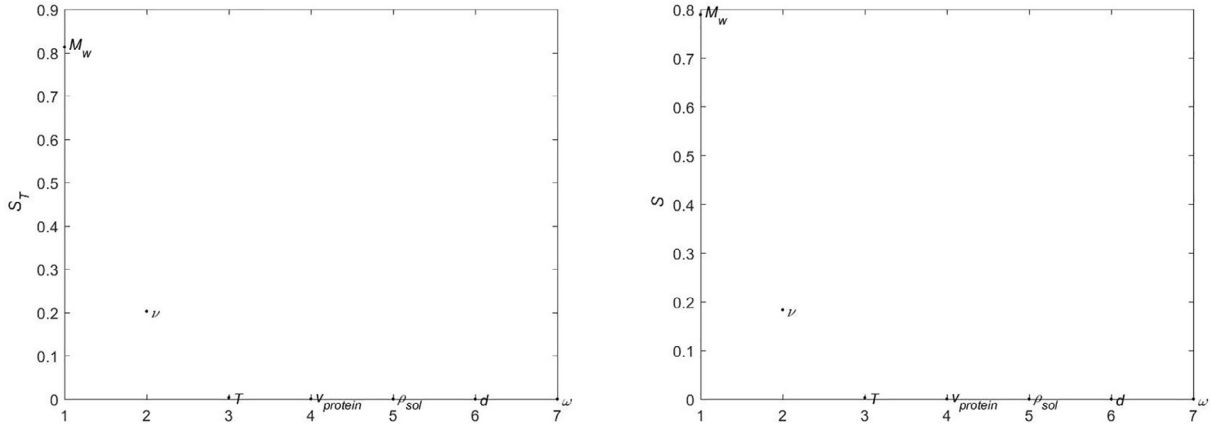

Fig. 9. GSA results for the diffusion velocity: *Si* (Right) and S_{Ti} (Left). *Si* indicates the actual fraction of variance accounted for by each factor (Homma and Saltelli, 1996), whereas S_{Ti} represents the total effect of factor *i*, i.e. the sum of the first order effects and all interactions with other factors.

ADH solution. In this way solutions with 80, 50, 30 and 20% remaining activity were prepared. No deviations greater than 8.11% could be observed when the measured activities were compared with the theoretical activities. In addition, no remaining activity could be observed when the activity of a completely denatured solution was measured. Results are shown in Table 5. The results make clear that the assay is suitable for this study.

4.4.2. ADH case

Three 10R vials, filled with 3 mL of a 1 mg mL^{-1} ADH solution, were subjected to a specific shear condition by rotating the vials around their longitudinal axis for 2 minutes at 2900 rpm or for 4 minutes at 800 or for 4 minutes at 400 rpm. Hence, according to Eq. (4) and (5) ADH was subjected to worst case shear rates of 2145 s^{-1}, 591 s^{-1} and 295 s^{-1} respectively. The current experimental spin freezing set-up does not allow to expose samples to higher shear rates, as the rotation velocity of the system is currently limited to 2900 rpm. It is important to note that the difference in shear rate when a 10R vial rotates at 2900 rpm ($\gamma = 2145\ s^{-1}$) or when a 10R vial rotates at 5729 rpm (i.e. $\gamma = 4238\ s^{-1}$) is relative small in comparison with other shear rates represented in Table 4. Hence, these conditions are not expected to have a different effect on the stability of ADH.

The activities of the rotated ADH solutions are compared with the activity of a control solution that is not subjected to any shear force. As represented in Table 6, no significant loss in activity is observed for ADH solutions exposed to shear in comparison with the control solution. DLS was used to compare the hydrodynamic diameter of ADH in solution before and after exposure to shear. As presented in Fig. 5, volume distributions of the hydrodynamic diameter of ADH in solution do not reveal any difference between the control solution and the stressed solutions. No (permanent) aggregates were formed after exposure to shear since no difference in average hydrodynamic diameter was detected in comparison with a non-stressed ADH solution. This confirms the results from the activity assay. The stability of ADH was not altered as a consequence of the shear stresses developed during spin freezing.

4.5. Sedimentation and diffusion during spin freezing

RCF start to develop when a vial rotates, hence causing sedimentation. Fig. 6 represents the generated RCF which are associated with the required rotation velocity to obtain a certain ΔL_{Rel}. Fig. 6 illustrates that the generated RCF is notable higher for 4R and 15R vials in comparison with the other vial types. Moreover, all other vial types possess comparable RCF values, especially for rotation velocities that involve maximum differences in average layer thickness above 5%. The RCF values associated with the rotation velocity that is required to achieve a maximum ΔL_{Rel} of 5% are represented in Table 3. These RCF values are low in comparison with typically used RCF values (7000 g up to 800,000 g) for centrifugation and ultracentrifugation, respectively. This is already a first indication that sedimentation will be very limited during the time frame of the spin freezing step. However, the sedimentation velocity of biopharmaceuticals will be determined to check the influence of centrifugal forces and thus sedimentation.

Firstly, the sedimentation velocity of ADH will be determined in order to examine the relevance of sedimentation of proteins during spin

freezing. The volume of ADH with molecular weight M_w = 150 kg mol^{-1} was calculated with Eq. (9). This results in a volume of $1.81\,10^{-25}\,m^{-3}$. Furthermore this implies that the minimal radius is $3.51\,10^{-9}$ m.

For an aqueous ADH solution with a viscosity of $1.016\,10^{3}$ kg m^{-1} s^{-1} and a density of 990.8 kg m^{-3} (i.e. the viscosity and density of water at 293 K) a sedimentation coefficient of 10.18 Svedberg was obtained according Eq. (8). One Svedberg is defined as 10^{-13} s.

As represented in Table 3, the highest RCF value, and thus sedimentation velocity, is achieved for a 4R vial when a maximum relative difference of 5% in frozen product layer thickness is desired. Based on Eq. (7) this results in a sedimentation velocity of $6.59\,10^{-9}$ m s^{-1} when the vial rotates at 9181 rpm and with d = 0.007 m (i.e. radius of a 4R vial). It is obvious that this low sedimentation velocity indicates that sedimentation of proteins is not an issue during spin freezing.

Besides the sedimentation velocity, the diffusion velocity was determined to check the relevance of diffusion during spin freezing. This was achieved by calculating the diffusion constant D according Eq. (11).

This results in a diffusion coefficient of $6.10\,10^{-11}$ m^2 s^{-1} at 293 K. This low diffusion coefficient implies that diffusion is not relevant, since it cannot cause a relevant separation between excipients and proteins during the time frame (maximum 10 min) of spin freezing. It is important to realize that this is the diffusion and sedimentation distance at 293 K. Nevertheless the temperature of the solution will drop below 273 K at the end of the freezing step. As defined in Eq. (8) and Eq. (11) the sedimentation and diffusion velocity will reduce gradually with the decrease in temperature during freezing. This implies that sedimentation and diffusion become even more irrelevant at the end of the spin freezing step.

Secondly the sedimentation velocity of viruses was evaluated. The influenza virus, a large virus, has a sedimentation coefficient of 700 Svedberg (Data obtained from literature (Lief and Henle, 1956; Friedewald and Pickels, 1944)). The sedimentation velocity is determined for a 4R vial rotating at 9181 rpm (i.e. the velocity resulting in a maximum difference of 5% in layer thickness). This results as defined by Eqs. (7) and (12) to a sedimentation velocity of $1.15\,10^{-6}$ m s^{-1} at 293 K. This sedimentation velocity is 5730 times higher than the sedimentation velocity of proteins and has to be taken into account in order to limit intra-frozen product layer inhomogeinity caused by sedimentation. According to Eq. (1), a frozen product layer thickness of 1.16 mm is achieved when a 4R vial is filled with 1.5 mL of the virus formulation (i.e. one fourth of the overflow capacity). This implies that complete solidification (i.e. ice formation) should be achieved in 50 s, if the maximum tolerated sedimentation distance in the frozen product layer is 5% of the total layer thickness. Frozen product layer inhomogeneity will be greater than 5% if solidification is not completed within 50 s.

Thirdly, the sedimentation velocity for bacteria was determined. For all calculations was assumed that bacteria have a buoyant mass (Mb) ranging from $5\,10^{-18}$ kg up to $800\,10^{-18}$ kg and a radius of $2\,10^{-6}$ m. The sedimentation velocity was calculated for 20R and 4R vial (i.e. vial type associated with the lowest and highest RCF respectively, as stated in Table 3) is represented in Table 7. Fig. 7 represents the required time to reach the maximum allowed sedimentation distance (i.e. distance which causes a maximum frozen product layer inhomogeneity of 5%) for different buoyant masses. The frozen product layer inhomogeneity is larger than 5% if solidification is not achieved before the represented times in Fig. 7. In contrast, the diffusion constant of bacteria is $6.45\,10^{-10}$ m^2 s^{-1} at 293 K according to Eq. (13) and is therefore comparable with the diffusion velocity of proteins and is therefore not a limiting factor.

4.6. Global sensitivity analysis and uncertainty analysis

GSA is used to detect which parameter(s) have a significant influence on the sedimentation and diffusion velocity. A value close to zero for the first order indice or the total order indice indicates that a factor has no significant influence on the output variable.

Based on the GSA for the sedimentation velocity as output variable (Fig. 8), it can be concluded that the rotation velocity (ω), molecular weight of the protein (Mw), distance to the axis of rotation (d) and the viscosity (ν) are the most critical parameters. All other factors have (almost) no influence on the sedimentation velocity. As the difference in ranking for the first order and the total order indices is identical, the factors are (almost) not involved in interactions with other factors (which is also an indication for the linearity of the model). The fact that rotation velocity (ω) and distance to the axis of rotation (d) are critical factors can be explained since the sedimentation velocity depends on the amount of centrifugal forces that are developed during rotation. These forces are expressed by RCF, which according to Eq. (6), depends therefore on the rotation velocity (ω) and the inner radius of the vial (d). The molecular weight (Mw), the second most important parameter with a significant influence on the sedimentation velocity depends on the used protein. UA pointed out that even for a large protein, like IgM, the sedimentation velocity (m s^{-1}) is limited to: $[1.32\,10^{-8}; 4.86\,10^{-8}]$ ($p<0.05$) at the most extreme setting of 9181 rpm (i.e. the rotation velocity for a 4R vial that results in a maximum of 5% ΔL_{Rel}). Therefore it can be concluded that the sedimentation velocity is under control and remains negligible, even for large proteins (e.g. antibodies). In addition, a GSA and UA were performed for the diffusion velocity of proteins. As presented in Fig. 9, the GSA indicated that the molecular weight (Mw) and the viscosity of the formulation (ν) are critical parameters. As the viscosity (ν) continuously increases during spin freezing, diffusion will reduce during spin freezing. The molecular weight depends on the freeze-dried protein.

The uncertainty interval ($p < 0.05$) of IgM obtained during the UA: $[1.82\,10^{-11}; 3.15\,10^{-11}]$ highlighted that the diffusion velocity ($m^2\,s^{-1}$) is, even for large proteins, too low to cause separation between stabilizer and proteins.

5. Conclusion

The rotation velocity to obtain a desired ΔL_{Rel} is calculated for different vial types. A mechanistic approach suggested that the generated shear rate during spin freezing has no effect on the stability of proteins. This is confirmed experimentally since no loss of ADH activity is observed after longitudinal rotation of vials filled with an ADH solution, and thus exposure to shear. In addition, measurement of the hydrodynamic diameter via DLS, showed that no permanent aggregates are formed during this rotation step. Furthermore, the shear rate, generated during rotation of the vials, is comparable and even lower than other typically upstream process steps applied during the manufacturing of biopharmaceuticals. Calculations proved that sedimentation velocity is negligible for proteins and can be therefore ignored. In contrast, a maximum solidification (i.e. ice formation) time has to be taken into account for viruses and bacteria to avoid intra-frozen product layer inhomogeneity caused by sedimentation since their sedimentation velocity is relatively high in comparison with proteins. The diffusion velocity is too low to cause inhomogeneity in the product layer during the time frame of spin freezing and is therefore not relevant. The performed UA illustrates that the sedimentation and diffusion velocity of proteins is negligible for the total duration of the spin freezing step.

GSA revealed that the viscosity is a critical parameter for the sedimentation and diffusion velocity. This is interesting since the viscosity increases during spin freezing and is inversely proportional with the sedimentation and diffusion velocity, which implies that both velocities decrease during spin freezing.

References

Anné, J., Maldonado, B., Van Impe, J., Van Mellaert, L., Bernaerts, K., 2012. Recombinant protein production and streptomycetes. J. Biotechnol. 158 (4), 159–167. http://dx.

doi.org/10.1016/j.jbiotec.2011.06.028.
Ashton, L., Dusting, J., Imomoh, E., Balabani, S., Blanch, E.W., 2009. Shear-induced unfolding of lysozyme monitored in situ. Biophys. J. 96 (10), 4231–4236. http://dx.doi.org/10.1016/j.bpj.2009.02.024.
Bee, J.S., Stevenson, J.L., Mehta, B., Svitel, J., Pollastrini, J., Platz, R., Freund, E., Carpenter, J.F., Randolph, T.W., 2009. Response of a concentrated monoclonal antibody formulation to high shear. Biotechnol. Bioeng. 103 (5), 936–943. http://dx.doi.org/10.1002/bit.22336.
Bekard, I.B., Dunstan, D.E., 2009. Shear-Induced deformation of bovine insulin in couette flow. J. Phys. Chem. B 113 (25), 8453–8457. http://dx.doi.org/10.1021/jp903522e.
Bekard, I.B., Asimakis, P., Bertolini, J., Dunstan, D.E., 2011. The effects of shear flow on protein structure and function. Biopolymers 95 (11), 733–745. http://dx.doi.org/10.1002/bip.21646.
Brown, P.H., Balbo, A., Zhao, H., Ebel, C., Schuck, P., 2011. Density contrast sedimentation velocity for the determination of protein partial-specific volumes. PLoS ONE 6 (10). http://dx.doi.org/10.1371/journal.pone.0026221.
Brückl, L., Schröder, T., Scheler, S., Hahn, R., Sonderegger, C., 2016. The effect of shear on the structural conformation of rhGH and IgG1 in free solution. J. Pharm. Sci. 105 (6), 1810–1818. http://dx.doi.org/10.1016/j.xphs.2016.03.020.
Campolongo, F., Saltelli, A., Cariboni, J., 2011. From screening to quantitative sensitivity analysis. A unified approach. Comput. Phys. Commun. 182 (4), 978–988. http://dx.doi.org/10.1016/j.cpc.2010.12.039.
Cole, J.L., Lary, J.W., Moody, T., Laue, T.M., 2009. Analytical ultracentrifugation: sedimentation velocity and sedimentation equilibrium. Methods Cell Biol. 84 (07), 143–179. http://dx.doi.org/10.1016/S0091-679X(07)84006-4.Analytical.
Colombié, S., Gaunand, A., Lindet, B., 2001. Lysozyme inactivation under mechanical stirring: effect of physical and molecular interfaces. Enzyme Microb. Technol. 28 (9–10), 820–826. http://dx.doi.org/10.1016/S0141-0229(01)00340-4.
Corver, J., 2013. Method and system for freeze-drying injectable compositions. In: Particular pharmaceutical.
Davis, R., 2001. Crossflow microfiltration with backpulsing. In: Wang, W. (Ed.), Membrane separations in biotechnology, 2nd ed. Marcel Decker, New York, pp. 161–188 (Ch. Crossflow).
De Meyer, L., Van Bockstal, P.J., Corver, J., Vervaet, C., Remon, J.P., De Beer, T., 2015. Evaluation of spin freezing versus conventional freezing as part of a continuous pharmaceutical freeze-drying concept for unit doses. Int. J. Pharm. 496 (1), 75–85. http://dx.doi.org/10.1016/j.ijpharm.2015.05.025.
De Meyer, L., Lammens, J., Mortier, S.T.F., Vanbillemont, B., Van Bockstal, P.J., Corver, J., Nopens, I., Vervaet, C., De Beer, T., 2017. Modelling the primary drying step for the determination of the optimal dynamic heating pad temperature in a continuous pharmaceutical freeze-drying process for unit doses. Int. J. Pharm. 532 (1), 185–193. http://dx.doi.org/10.1016/j.ijpharm.2017.09.004.. URLhttp://linkinghub.elsevier.com/retrieve/pii/S0378517317308505.
Erickson, H.P., 2009. Size and shape of protein molecules at the nanometer level determined by sedimentation, gel filtration, and electron microscopy. Biolog. Proced. 11 (1), 32–51. http://dx.doi.org/10.1007/s12575-009-9008-x.
Franks, F., 1998. Freeze-drying of bioproducts: Putting principles into practice. Eur. J. Pharm. Biopharm. 45 (3), 221–229. http://dx.doi.org/10.1016/S0939-6411(98)00004-6.
Friedewald, W.F., Pickels, E.G., 1944. Centrifugation and ultrafiltration studies on allantoic fluid preparations of influenza virus. J. Exp. Med. 79 (3), 301–317. http://dx.doi.org/10.1084/jem.79.3.301.. URLhttp://www.pubmedcentral.nih.gov/articlerender.fcgi?artid=2135374&tool=pmcentrez&rendertype=abstract.
Frokjaer, S., Otzen, D.E., 2005. Protein drug stability: a formulation challenge, Nature reviews. Drug Discovery 4 (4), 298–306. http://dx.doi.org/10.1038/nrd1695.
Gomme, P.T., Hunt, B.M., Tatford, O.C., Johnston, A., Bertolini, J., 2006. Effect of lobe pumping on human albumin: investigating the underlying mechanisms of aggregate formation 1 (111), 103–111. http://dx.doi.org/10.1042/BA20050147.
Harpaz, Y., Gerstein, M., Chothia, C., 1994. Volume changes on protein folding. Structure (London, England: 1993) 2 (7), 641–649. http://dx.doi.org/10.1016/S0969-2126(00)00065-4.
Homma, T., Saltelli, A., 1996. Importance measures in global sensitivity analysis of nonlinear models. Reliab. Eng. Syst. Saf. 52, 1–17. http://dx.doi.org/10.1016/0951-8320(96)00002-6.
Jaspe, J., Hagen, S.J., 2006. Do protein molecules unfold in a simple shear flow? Biophys. J. 91 (9), 3415–3424. http://dx.doi.org/10.1529/biophysj.106.089367.
Kasper, J.C., Friess, W., 2011. The freezing step in lyophilization: physico-chemical fundamentals, freezing methods and consequences on process performance and quality attributes of biopharmaceuticals. Eur. J. Pharm. Biopharm. 78 (2), 248–263. http://dx.doi.org/10.1016/j.ejpb.2011.03.010.
Kroll, M., 1996. Platelets and shear stress. J. Am. Soc. Hematol. 86 (5), 1525–1541.
Le Roy, A., Wang, K., Schaack, B., Schuck, P., Breyton, C., Ebel, C., 2015. AUC and small-angle scattering for membrane proteins. Methods Enzymol. 562, 257–286. http://dx.doi.org/10.1016/bs.mie.2015.06.010.
Lief, F.S., Henle, W., 1956. Studies on the soluble antigen of influenza virus. Virology 2 (6), 782–797. http://dx.doi.org/10.1016/0042-6822(56)90058-7.
Maa, Y.-F., Hsu, C.C., 1997. Protein denaturation by combined effect of shear and air-liquid interface. Biotechnol. Bioeng. 54 (6), 503–512. http://dx.doi.org/10.1002/(SICI)1097-0290(19970620)54:6503::AID-BIT13.0.CO;2-N.
McKay, M., Beckman, R., Conover, W., 2000. A comparison of three methods for selecting values of input variables in the analysis of output from computer code. Technometrics 42, 55–61.
Mok Y., 2006. Sedimentation Velocity Analysis of Amyloid Oligomers and Fibrils, Amyloid, Prions, and Other Protein Aggregates, Part C 413(06), 2006, pp. 199–217. doi:10.1016/S0076-6879(06)13011-6. URL http://ovidsp.ovid.com/ovidweb.cgi?T=JS&PAGE=reference&D=emed7&NEWS=N&AN=2006495263.
Mortier, S.T.F.C., Gernaey, K.V., De Beer, T., Nopens, I., 2014. Global sensitivity analysis applied to drying models for one or a population of granules. AIChE J. 60 (5), 1700–1717. http://dx.doi.org/10.1002/aic.14383.
Oliva, A., Santoveña, A., Fariña, J., Llabrés, M., 2003. Effect of high shear rate on stability of proteins: kinetic study. J. Pharm. Biomed. Anal. 33 (2), 145–155. http://dx.doi.org/10.1016/S0731-7085(03)00223-1.
Pikal, M.J., 2002. Freeze Drying. Encycl. Pharm. Technol. 1299–1326. http://dx.doi.org/10.1016/0042-207X(52)90503-4.
Saltelli, A., 2006. The critique of modelling and sensitivity analysis in the scientific discourse. An overview of good practices, Washington.
Singh, I., Themistou, E., Porcar, L., Neelamegham, S., 2009. Fluid shear induces conformation change in human blood protein von Willebrand factor in solution. Biophys. J. 96 (6), 2313–2320. http://dx.doi.org/10.1016/j.bpj.2008.12.3900.
Squire, P.G., Himmel, M.E., 1979. Hydrodynamics and protein hydration. Arch. Biochem. Biophys. 196 (1), 165–177. http://dx.doi.org/10.1016/0003-9861(79)90563-0.
Stroev, P.V., Hoskins, P.R., Easson, W.J., 2007. Distribution of wall shear rate throughout the arterial tree: A case study. Atherosclerosis 191 (2), 276–280. http://dx.doi.org/10.1016/j.atherosclerosis.2006.05.029.
Thomas, C.R., Dunnill, P., 1979. Action of shear on enzymes: studies with catalase and urease. Biotechnol. Bioeng. 21 (12), 2279–2302. http://dx.doi.org/10.1002/bit.260211209.
Thomas, C.R., Geer, D., 2011. Effects of shear on proteins in solution. Biotechnol. Lett. 33 (3), 443–456. http://dx.doi.org/10.1007/s10529-010-0469-4.
US FDA, ICH Q8 (R2) PAT guideline, 2009.
Van Bockstal, P.-J., 2016. Mechanistic modelling of infrared mediated energy transfer during the primary drying step of continuous freeze-drying process. Eur. J. Pharm. Biopharm. 114, 1–17. http://dx.doi.org/10.1016/j.ejpb.2017.01.001.
Van Bockstal, P.-J., De Meyer, L., Corver, J., Vervaet, C., De Beer, T., 2016. Noncontact infrared-mediated heat transfer during continuous freeze-drying of unit doses. J. Pharm. Sci. 1–12. http://dx.doi.org/10.1016/j.xphs.2016.05.003.
Virkar, P.D., Narendranathan, T.J., Hoare, M., Dunnill, P., 1981. Studies of the effect of shear on globular proteins: extension to high shear fields and to pumps. Biotechnol. Bioeng. 23 (2), 425–429. http://dx.doi.org/10.1002/bit.260230216.
Walstra, P., 2001. Effect of agitation on proteins. In: Dickinson, E., Miller, R. (Eds.), Food Colloids: Fundamentals of Formulation. Royal society of Chemistry, pp. 245–254.
Wang, W., 2000. Lyophilization and development of solid protein pharmaceuticals. Int. J. Pharm. 203. http://dx.doi.org/10.1016/S0378-5173(00)00423-3.
Wilkes, J., 2006. Fluid Mechanics for Chemical Engineers. Pearson Education.